Processing and Application of Ceramics 12 [4] (2018) 383–393
https://doi.org/10.2298/PAC1804383P

BY-NC-ND

Structure and electrical properties of $(Bi,Na)_{0.94}Ba_{0.06}Ti_{1-x}(Mg_{1/3}Nb_{2/3})_xO_3$ ceramics

Ashutosh Prasad[1,*], Ranjan Kumar Mishra[2], Kumar Prabhat Chandra[3], Kamal Prasad[1]

[1]*UniversityDepartment of Physics, T.M. Bhagalpur University, Bhagalpur, 812007, India*
[2]*Department of Physics, Bhagalpur College of Engineering, Bhagalpur, 813210, India*
[3]*Department of Physics, S. M. College, Bhagalpur, 812001, India*

Received 15 June 2018; Received in revised form 17 October 2018; Accepted 9 December 2018

Abstract

In this work the effect of pseudo-cation $(Mg^{2+}_{1/3}Nb^{5+}_{2/3})^{4+}$ addition on Ti-site of $(Bi_{0.5}Na_{0.5})_{0.94}Ba_{0.06}TiO_3$ ceramics, having general formula $(Bi,Na)_{0.94}Ba_{0.06}Ti_{1-x}(Mg_{1/3}Nb_{2/3})_xO_3$ ($0 \leq x \leq 1$), on their structural and electrical properties was investigated. These compounds were prepared using a standard high temperature solid-state reaction technique and characterized by structural, microstructural, impedance, and conductivity studies. The sintered ceramics are almost phase-pure perovskite materials showing high bulk densities (>95% TD), uniform microstructure and satisfactory impedance properties in all the samples. Besides, an attempt has been made to ascertain the role of grains and grain boundaries on the electrical properties of these solid solutions and their dependence on the temperature and frequency, using complex impedance spectroscopy technique. The obtained data analysed in the framework of AC conductivity, complex impedance as well as electric modulus formalisms indicate on dominant negative temperature coefficient of resistance (NTCR) character of the materials due to the contribution of semiconducting grains. Further, the dielectric relaxation in the material was seen to be of non-Debye type.

Keywords: *perovskites, lead-free, ceramics, dielectric, impedance, microstructure*

I. Introduction

Lead-based piezoelectric ceramics have been widely used for many decades in actuators, sensors and transducers because of their excellent electrical properties [1]. Perovskite-type oxides like $Pb(Mg_{1/3}Nb_{2/3})O_3$, $Pb(Zn_{2/3}Nb_{1/3})O_3$ and $Pb(Zr,Ti)O_3$ have been shown extremely useful for a variety of applications in ferroelectric and piezoelectric devices [2]. Most of these materials are lead-based with more than one cation occupying the octahedral lattice sites. The presence of heterovalent ions with different ionic radii, valence states and varying polarizabilities in the octahedral site were found to be effective in enhancing the dielectric, electrical and electromechanical properties. However, the toxicity of lead and volatilization of toxic PbO during processing of these materials have given rise to an increasing demand for alternative environment-friendly materials having comparable dielectric, electrical and electromechanical properties to the lead-based materials.

Bismuth sodium titanate (BNT), a perovskite material with the Curie temperature $T_C = 320\,°C$, remnant polarization $P_r = 38\,\mu C/cm^2$ and coercive field $E_c = 73\,kV/cm$, as reported by Smolenskii *et al.* [3], has been projected as a potential candidate in place of the lead-based piezoelectric ceramics. Nevertheless, the electrical properties of the BNT ceramics are not comparable to those of lead-based piezoelectric ceramics. It has further been reported that BNT-based compositions modified with $BaTiO_3$, $NaNbO_3$, $BiFeO_3$, $Bi_2O_3 \cdot Sc_2O_3$ or La_2O_3 showed improved piezoelectric properties and easier treatment in poling process compared with the pure BNT ceramics [4–9]. Takenaka [10] reported that BNT-based solid solutions with a rhombohedral-tetragonal morphotropic phase boundary (MPB) composition showed better piezoelectric and pyroelectric properties when compared with unmodified BNT ceramics. It has also been reported that the composition close to the MPB has relatively good piezoelectric and dielectric properties after the addition of 6 mol%

* Corresponding authors: tel: +91 9470627940,
e-mail: *apd.phy@gmail.com*

of $BaTiO_3$ in BNT [11–14]. Lead-free bismuth sodium titanate-sodium niobate (BNT-NN), $(Bi_{0.5}Na_{0.5})TiO_3$-$NaNbO_3$ ceramics were prepared by Li *et al.* [15] using the conventional high-temperature solid-state reaction technique. They concluded that d_{33} increased from 64 to 88 pC/N when 2 mol% of $NaNbO_3$ was added and then decreased gradually. However, the dielectric constant was seen to increase gradually with the increase in $NaNbO_3$ content. This was attributed to the co-effect of the soft additive Nb^{5+} ion doping at B-site and hard additive Na^+ ion doping at A-site. Another interesting system is bismuth sodium titanate (BNT) ceramics mixed with $KNbO_3$ (KNN). It was shown that the fabricated ceramics are orthorhombic up to 2 mol% BNT, tetragonal up to 9 mol% BNT, cubic up to 20 mol% BNT and rhombohedral thereafter [16]. KNN mixed with 2 mol% BNT, regarded as an MPB composition, has $d_{33} \sim 195$ pC/N and the Curie temperature ~395 °C [16].

BNT exhibited relaxor behaviour with a less temperature stable dielectric constant [17]. Therefore, several additional studies have been reported pertaining to the enhancement of its ferroelectric properties by forming solid solutions of BNT with $K_{0.5}Bi_{0.5}TiO_3$ [18], $Ba(Ti,Zr)O_3$ [19], $Bi(Mg_{1/3}Nb_{2/3})O_3$ [20], $BiFeO_3$ [21] as well as with cations of rare earth and transition metal ions like Ce^{4+} [22], Mn^{4+} [23], La^{3+} [24], Fe^{3+} [25] and Nb^{5+} [26]. Among the various systems that have been reported, bismuth sodium barium titanate $(Bi_{0.5}Na_{0.5})_{1-x}Ba_xTiO_3$ (BNBTx) solid solution that exhibited a morphotropic phase boundary (MPB) near x = 0.06 showed relatively enhanced piezoelectric properties.

Recent reports showed the successful formation of solid solutions of $Ba(Fe_{1/2}Ta_{1/2})O_3$ [27] or $NaNbO_3$ [28,29] with $(Bi_{0.5}Na_{0.5})_{0.94}Ba_{0.06}TiO_3$ (BNBT6) which showed giant dielectric constant. In another study, the effect of pseudo-cation $(Mg_{1/3}Nb_{2/3})^{4+}$ substitution on the phase transition behaviour of BNBT6 was studied [30]. Our extensive literature survey indicated that no attempt has so far been made to characterize the electrical properties of $(Mg^{2+}_{1/3}Nb^{5+}_{2/3})$ substituted $(Bi_{0.5}Na_{0.5})_{0.94}Ba_{0.06}TiO_3$ ceramics using impedance spectroscopy technique. It is well-known that the inhomogeneous composition due to the doping element and internal stress within the microstructure are matters of concern because they greatly influence the electrical properties. The present study has been undertaken with these views in mind. When Ti^{4+} sites with the ionic radius (R_{Ti}) of 0.605 Å are substituted by Mg^{2+} ion (R_{Mg} = 0.72 Å) and Nb^{5+} ion (R_{Nb} = 0.64 Å), the two substitutions are supposed to give rise to different effects. The larger ion Mg^{2+} occupies more space, leading to the decrease in rattling space for the cations at the centre of oxygen octahedra, while the smaller ion Nb^{5+} occupies almost the same space as had been previously occupied by Ti^{4+}. $(Mg_{1/3}Nb_{2/3})^{4+}$ has an average radius of 0.67 Å, which is close to that of Ti^{4+}. Therefore, $(Mg_{1/3}Nb_{2/3})^{4+}$ ion should enter into the six-fold coordinated B-site of the perovskite structure to substitute Ti^{4+} because of radius matching, which may lead to the increase of lattice dimensions. It is, therefore, believed that as $(Mg^{2+}_{1/3}Nb^{5+}_{2/3})$ may possess a different state than that of Ti^{4+} (3d) and the introduction of $(Mg^{2+}_{1/3}Nb^{5+}_{2/3})$ would bring in a different valence band distance from that of Ti–O, thereby leading to the enhancement of the electrical properties.

Hence, the present work is undertaken to investigate the effect of substitution of $(Mg_{1/3}Nb_{2/3})^{4+}$ at B-site of BNBT6, on the microstructure, phase transition temperatures, impedance, and electrical conductivity. The main goal was to have insight into the relaxation mechanism and defects relation in these materials and to see whether the substitution brings into any significant improvement in any of its electrical properties having their practical and industrial applications. The nature of charge transport taking place via different modes such as dipole reorientation, charge displacement and space charge formalism [31] has also been sought in the present study.

II. Experimental procedure

The starting materials were AR grade Bi_2O_3, $BaCO_3$, TiO_2, Na_2CO_3, MgO and Nb_2O_5. All compositions were prepared by conventional high-temperature solid-state reaction technique. Stoichiometric amounts of precursor powders corresponding to the compositions $(Bi,Na)_{0.94}Ba_{0.06}Ti_{1-x}(Mg_{1/3}Nb_{2/3})_xO_3$ (where x = 0.0, 0.25, 0.50, 0.75 and 1.00) were mixed in ethanol media and well ground in an agate mortar pestle. The mixed precursor powders with different compositions, i.e. x = 0.0, 0.25, 0.50, 0.75 and 1.00, were calcined at 1140, 1080, 1080, 1100 and 1125 °C, respectively (all for 4 h). The calcined powders were further ground with PVA as a binder. Cylindrical pellets having diameter ~10 mm and thickness ~1–2 mm were formed using the constituent powder samples by applying uniaxial pressure ~83 MPa for 5 min in hydraulic press. The pellets with different compositions, i.e. x = 0.0, 0.25, 0.50, 0.75 and 1.00, were sintered in a covered alumina crucible at 1160, 1100, 1100, 1120 and 1140 °C, respectively (all for 3 h). The optimal calcination temperatures for obtaining single phase compounds were found by XRD analyses. Similarly, the sintering temperatures were also optimised in order to achieve samples with densities higher than 90% TD. It was found that on increasing the temperature beyond the indicated limits, density of the samples decreased a bit because of the burnout of the volatile substances and the hot samples began to melt.

Phase formation was checked using an X-ray diffractometer (Bruker D8 Advance) at room temperature, using CuK_α radiation (λ = 1.5405 Å), for 2θ between 20° and 70°. The unit cell structure and dimensions, *hkl* values, and space group of all the specimens were obtained using the FullProf software. The surface mor-

phology of fractured surfaces of all the sintered specimens was obtained by scanning electron microscope (SEM, EVO 18, Carl Zeiss Microscopy Ltd., UK). ImageJ software was used to estimate grain sizes. For impedance measurements, a silver paste was coated on the polished surface of the pellets and fired at 600 °C for 30 min. Impedance analyser (E4990A-120, Keysight Technologies, USA) was used to measure the complex impedance and phase angle in frequencies ranging from 100 Hz to 10 MHz and temperatures from 20–500 °C using heating and cooling rates of 5 °C/min. Hereinafter, compositions with x = 0.0, 0.25, 0.50, 0.75 and 1.00 in $(Bi_{0.5}Na_{0.5})_{0.94}Ba_{0.06}Ti_{1-x}(Mg_{1/3}Nb_{2/3})_xO_3$ will be denoted as BNBT-MN_0, BNBT-$MN_{0.25}$, BNBT-$MN_{0.50}$, BNBT-$MN_{0.75}$ and BNBT-$MN_{1.00}$, for brevity sake.

III. Results and discussion

3.1. Structure

XRD patterns of the pure BNBT6 and $(Bi_{0.5}Na_{0.5})_{0.94}Ba_{0.06}Ti_{1-x}(Mg_{1/3}Nb_{2/3})_xO_3$ samples with x = 0.25, 0.50, 0.75 and 1.00 are shown in Fig. 1 (it depicts the Rietveld refined XRD plots of BNBT-MN_x ceramics). The appearance of single and sharp peaks and absence of secondary peaks characteristics of constituent oxides and/or carbonates for each of the compounds indicated the formation of the single phase compounds and complete solubility of pseudo-cation $(Mg^{2+}_{1/3}Nb^{5+}_{2/3})$ into BNBT6 matrix, thus indicating the formation of homogeneous solid solutions. The XRD pattern analysis indicated that BNBT-MN_x (x = 0, 0.25 and 0.50) compositions have monoclinic structure while BNBT-$MN_{0.75}$ and BNBT-$MN_{1.00}$ have tetragonal structure resembling with almost pseudo-cubic (having only a small difference of ~0.001 Å between lattice parameters a and c at x = 1.0 with space group $P4/mmm$, Table 1). The changes in the intensity of peaks and peak positions are evident, thereby pointing towards a change in lattice parameters and crystal symmetry with the inclusion of $(Mg^{2+}_{1/3}Nb^{5+}_{2/3})$. Therefore, partial replacement of Ti^{4+} ion by pseudo-cation $(Mg^{2+}_{1/3}Nb^{5+}_{2/3})$ is seen to be responsible for the change in the basic unit cell structures of the solid-solutions. Expanded XRD plots for 2θ between the limiting values of 44.5° and 47.5° are shown in Fig. 1b. They clearly manifest the peak splitting for tetragonal system and merger of the two peaks for pseudo cubic structure in which B-site

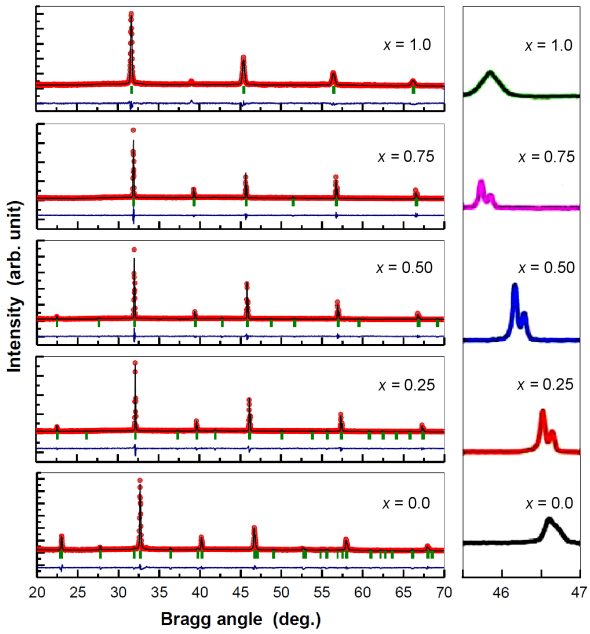

Figure 1. Rietveld refined XRD plots of BNBT-MN_x (x = 0, 0.25,0.50, 0.75 and 1.00) ceramics (a) and enlarged XRD pattern in 2θ range of 45.5°–47.5° (b)

Ti^{4+} is completely substituted by the pseudo cation $(Mg^{2+}_{1/3}Nb^{5+}_{2/3})^{4+}$.

Figure 2 illustrates the SEM micrographs of the fractured surfaces of sintered BNBT-MN_x ceramics ($0 \leq x \leq 1.0$). Nearly cuboid shaped grains of unequal sizes are seen to be densely distributed throughout the samples for all the compositions. Also, very few pores are observed. The sintered samples are almost phase-pure perovskite materials showing high relative densities (>95% TD) having uniform and dense microstructure (except for the sample BNBT-$MN_{1.00}$ which showed a bit lower relative density of ~90% TD). The minimum and maximum grain sizes for the ceramics having x = 0, 0.25, 0.50, 0.75, 1.0 are estimated to be 1.0–2.6, 3.2–10.0, 2.0–8.4, 16.0–30.0 and 1.4–4.0 μm, respectively. With increasing x, the grain size, as well as grain morphology of BNBT-MN_x ceramics, are seen to change considerably and the grain size is found to be maximal for x = 0.75 i.e composition where the phase change from monoclinic to tetragonal or pseudo-cubic could be identified. This effect indicates the dominance of semiconducting grains over insulating grain boundaries for the aforesaid ceramic composition.

Table 1. Lattice parameters and crystal structure of the $(Bi_{0.5}Na_{0.5})_{0.94}Ba_{0.06}Ti_{1-x}(Mg_{1/3}Nb_{2/3})_xO_3$ (x = 0, 0.25,0.50, 0.75 and 1.00) ceramics

Parameters	x = 0	x = 0.25	x = 0.50	x = 0.75	x = 1.0
Crystal System	Monoclinic	Monoclinic	Monoclinic	Tetragonal	Tetragonal
Space group	$P2m$ (10)	$P2m$ (10)	$P2m$ (10)	$P4/mmm$ (123)	$P4/mmm$ (123)
a [Å]	3.9908	3.9751	4.0450	2.8094	2.8241
b [Å]	3.8609	2.7816	2.8004	2.8094	2.8241
c [Å]	3.2943	3.4424	3.3029	3.9727	2.8251
β [°]	102.942	98.292	101.786	90.0	90.0
V [Å^3]	49.4691	37.6647	36.6242	31.3559	22.5326

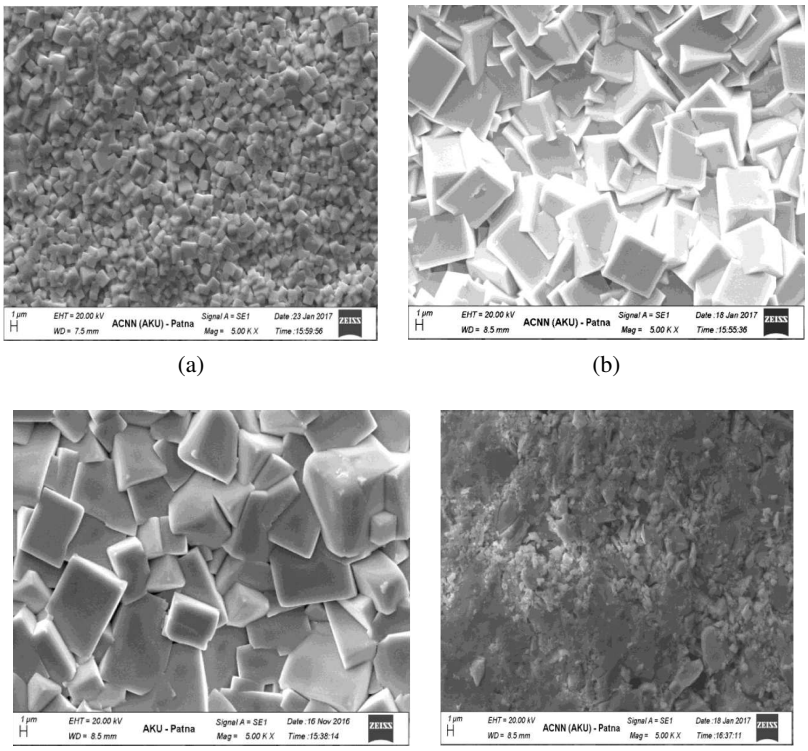

(a) (b)

(c) (d)

Figure 2. SEM micrographs of ceramic compositions $(Bi_{0.5}Na_{0.5})_{0.94}Ba_{0.06}Ti_{1-x}(Mg_{1/3}Nb_{2/3})_xO_3$ where x is: a) 0, b) 0.25, c) 0.50 and d) 1.00

3.2. Electric properties

The AC impedance analysis has been found to be a powerful tool to separate the grain boundary and grain-electrode effects, which usually are the sites of traps for oxygen vacancies and other defects. It is also useful in establishing space charge polarization and its relaxation mechanism, by aptly assigning different values of resistance and capacitance to the grain and grain boundary effects. A remarkable aspect of the impedance analysis is the option of calculating the different contributions to the conductivity, namely the bulk, grain boundary, and grain-electrode contributions.

Figures 3 and 4 show the $Z'(f)$ and $Z''(f)$ plots for BNBT-MN_0, BNBT-$MN_{0.25}$, BNBT-$MN_{0.50}$, BNBT-$MN_{0.75}$ and BNBT-$MN_{1.00}$, compositions at several temperatures between room temperature and 500 °C. It can be seen (Fig. 3a) that for the sample BNBT-MN_0 at lower temperatures Z' decreases monotonically with increasing frequency up to a certain limiting range (~10 kHz in the lower temperature range and ~100 kHz in the higher temperature range) above which it is almost frequency-independent. The higher values of Z' at lower frequencies and higher temperatures indicate that the polarization in the ceramics is larger. However, the doped BNBT-MN_x samples show almost constant Z' at low frequencies (Fig. 3b,c,d,f) up to a certain value after which appears that Z' merges together with continuous decrease. The temperature, at which this frequency-dependent to frequency-independent change in Z' occurs, slightly varies with frequency in the different material compositions. This also signifies that the resistive grain boundaries become conducting at these temperatures and that the grain boundaries are not relaxing even at the highest measurement ranges of frequency and temperature.

For the sample BNBT-MN_0 $Z''(f)$ plot (Fig. 4a) shows almost identical monotonically decreasing type of variation up to the same frequency limit ~100 kHz above which it is almost frequency-independent. However, the doped samples show dispersion at low frequencies (Fig. 4b,c,d,f) after which appears that Z'' merges together with continuous decrease, showing frequency-independent nature of variation extending up to the highest frequency limit at all chosen measurement temperatures. The observed merging of Z'' (as well as of Z') at higher frequencies for all the temperatures indicates possible release of space charges and their accumulation at the boundaries of homogeneous phases in the fabricated materials under the applied external field. At lower temperatures, a monotonic decrease of Z'' for all the compositions indicated that at lower temperatures the relaxation is absent in the material system. This means that relaxation species are immobile defects and the orientation effects may be associated. Further, the decreasing magnitudes of Z' and Z'' with increasing frequencies implied that relaxation in the materials is temperature-dependent, and apparently there is no single relaxation time.

In the Z'' vs. frequency plots (Fig. 4) it is shown that the Z'' values reach maxima (Z''_{max}) at higher tempera-

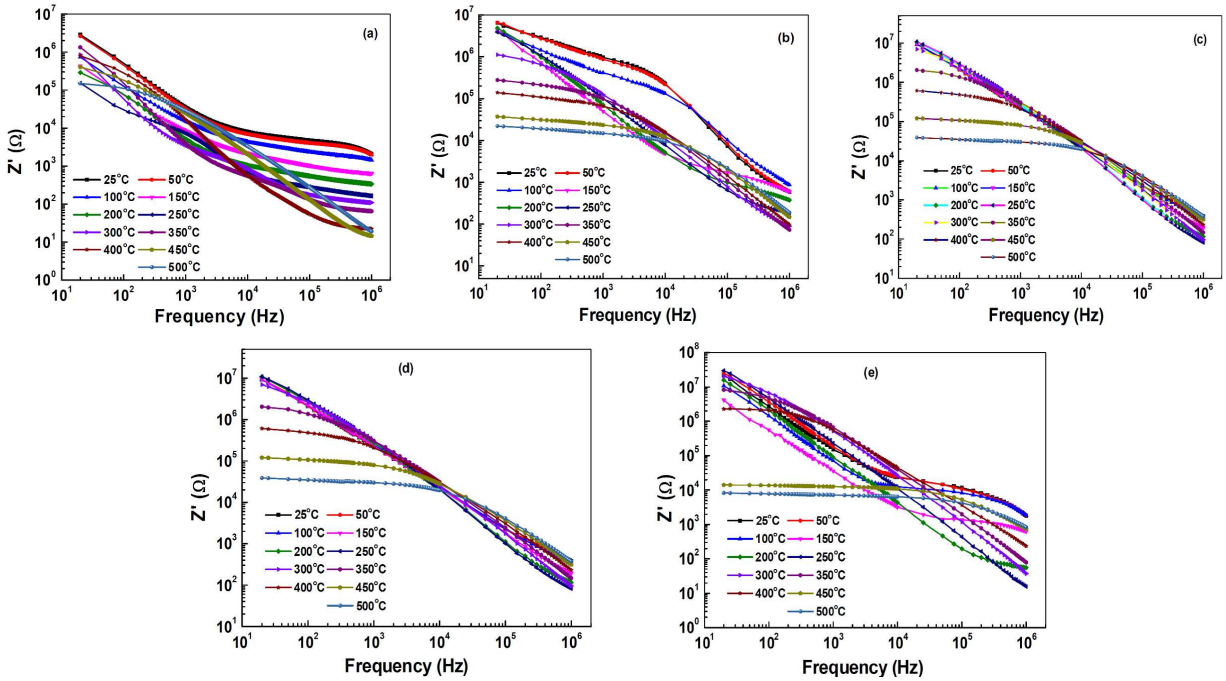

Figure 3. Frequency dependence of the real part of complex impedance for $(Bi_{0.5}Na_{0.5})_{0.94}Ba_{0.06}Ti_{1-x}(Mg_{1/3}Nb_{2/3})_xO_3$, where x is 0 (a), 0.25 (b), 0.50 (c), 0.75 (d) and 1.00 (e) at temperatures up to 500 °C

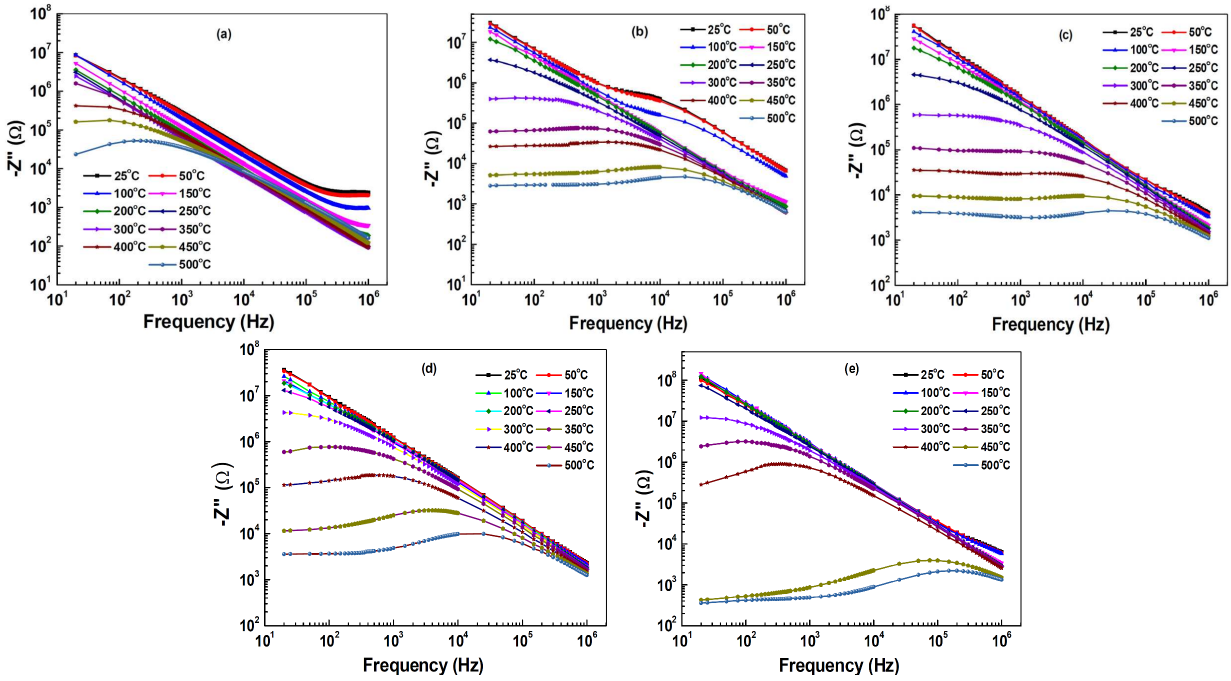

Figure 4. Frequency dependence of the imaginary part of complex impedance for $(Bi_{0.5}Na_{0.5})_{0.94}Ba_{0.06}Ti_{1-x}(Mg_{1/3}Nb_{2/3})_xO_3$, where x is 0 (a), 0.25 (b), 0.50 (c), 0.75 (d) and 1.00 (e) at temperatures up to 500 °C

tures and their positions are shifted towards higher frequency with an increase of temperature. This shift in the positions of the frequency maxima indicates active conduction through the grain boundary in the BNBT-MN_x ceramics. The magnitude of Z''_{max} also decreases with the increase in temperature. At higher frequencies, the dispersion due to the grain predominates due to the diminishing of the space charge effects, as the relaxation times of the grain boundaries are very high compared to those of grains. The diffuseness of $Z''(f)$ peak indicates the distribution of the relaxation frequency and the increase in full width at half Z''_{max} value with the increase of temperature indicates an increase of relaxation frequency distribution. The distribution of relaxation frequency in the investigated BNBT-MN_x samples may be attributed to cationic disorder due to the random distribution of B-site cations $(Mg_{1/3}Nb_{2/3})^{4+}$ and Ti^{4+} having different ionic radii and valence states.

Complex impedance spectroscopy (CIS) is a powerful tool for characterizing many of the electrical proper-

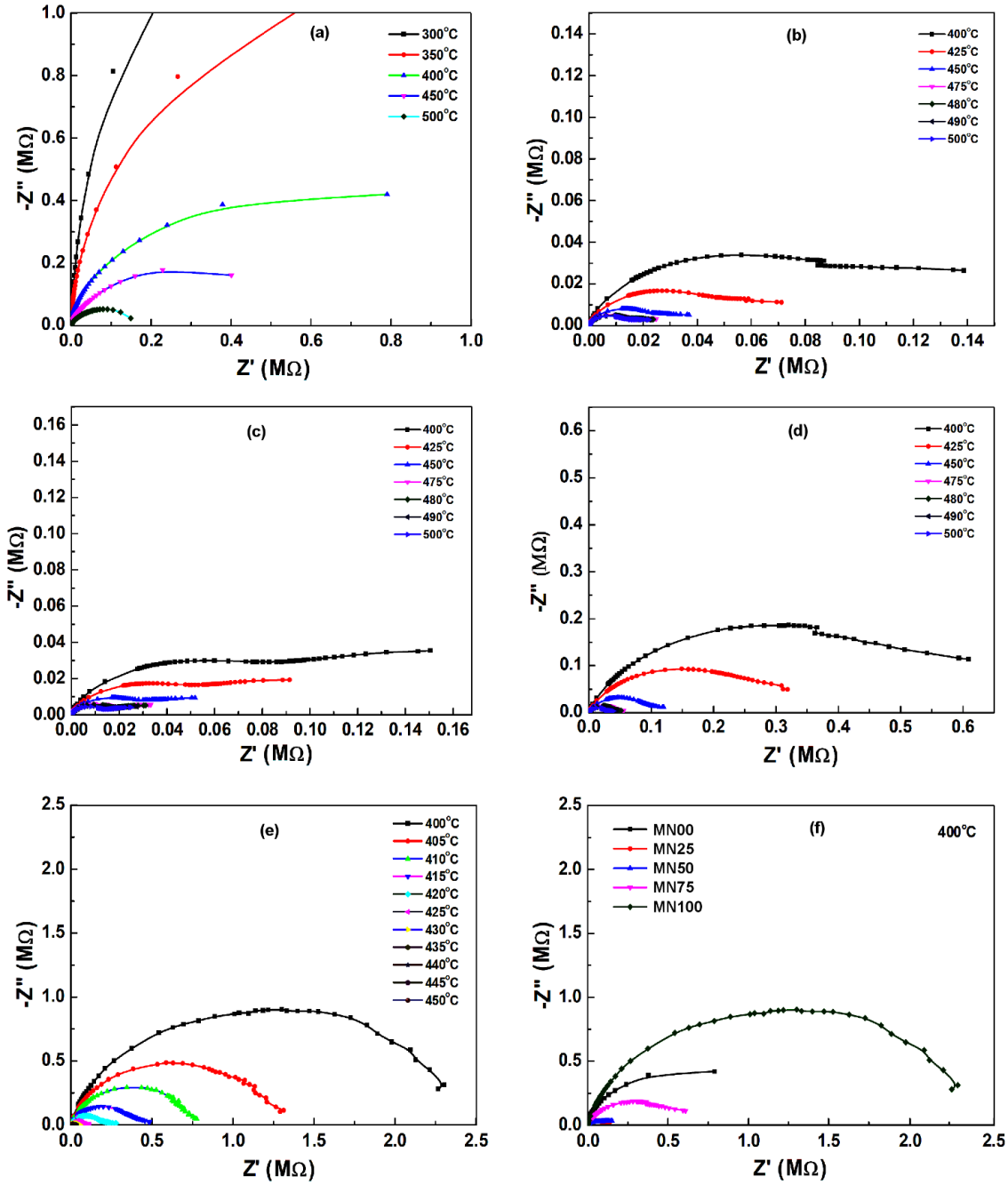

Figure 5. Complex impedance plots for $(Bi_{0.5}Na_{0.5})_{0.94}Ba_{0.06}Ti_{1-x}(Mg_{1/3}Nb_{2/3})_xO_3$ (x = 0, 0.25,0.50, 0.75 and 1.00) from 400 to 500 °C at different indicated temperatures. Figure (f) shows the complex impedance plots for the five compositions at 400 °C

ties of materials and their interfaces with electronically conducting electrodes. It may be used to investigate the dynamics of bound or mobile charges in the bulk or interfacial regions of any kind of solid or liquid material: ionic, semiconducting, mixed electronic-ionic, and even insulators (dielectrics). The CIS gives the direct correlation between the response of a real system and an idealized model circuit composed of discrete electrical components. An equivalent circuit based on the impedance and electric modulus spectra provides the physical explanation of the processes occurring inside a material system. Electrical AC data may be presented in any of the four interrelated formalisms: relative permittivity $\varepsilon^* = \varepsilon' + j \cdot \varepsilon''$; impedance $Z^* = Z' + j \cdot Z'' = 1/(j \cdot \omega \cdot C_0 \cdot \varepsilon^*)$; electric modulus $M^* = M' + j \cdot M'' = 1/\varepsilon^*$; admittance $Y^* = Y' + j \cdot Y'' = j \cdot \omega \cdot C_0 \cdot \varepsilon^*$; and $\tan\delta = \varepsilon''/\varepsilon' = M''/M' = Z'/Z'' = Y'/Y''$, where ω ($= 2\pi f$) is the angular frequency, C_0 ($= \varepsilon_0 \cdot A/t$) is the geometrical capacitance, $j = \sqrt{-1}$, ε_0 is the permittivity of free space (8.854×10^{-12} F/m), t and A are the thickness and area of the pellet, and δ is complementary to the phase angle (θ), as observed by the impedance analyser.

The Nyquist plots between $Z'(f)$ and $Z''(f)$ for all investigated ceramic compositions are observed at several temperatures between 400–500 °C (Fig. 5). The

impedance spectrum is distinguished by semicircles. A series array of parallel RC combination (R_g, C_g) in series with a resistor (R_s) (though almost frequency-independent data of R_s are not shown in any of the plots, for brevity sake) in parallel with combination (R_{gb}, C_{gb}) was found to best fit the experimental data for the given composition, thereby indicating the dominant contribution from intrinsic grains in the samples. The observed semicircles in the impedance Cole-Cole plots indicated a tendency to bend towards the abscissa with their centres below the real axis, having comparatively larger radii and the radii decreasing with increase in temperature. This indicates a decrease in resistivity with the increase of temperature i.e., representing the NTCR behaviour and distribution of relaxation times in the investigated BNBT-MN$_x$ samples with a clear cut departure from the ideal Debye type behaviour.

Complex modulus spectroscopy (CMS) analysis is an alternative approach to explore electrical properties of the material and magnify any other effects present in the sample (which are unidentifiable or superimposed one over the other in CIS technique) as a result of different relaxation time constants. It is an important and convenient tool to determine, analyse and interpret the dynamical aspects of electrical transport phenomena (i.e. parameters such as carrier/ion hopping rate, conductivity based relaxation time, etc.). In order to analyse and interpret the experimental data, it is essential to have a model equivalent circuit that provides a realistic representation of the electrical properties. The modulus representation suppresses the unwanted effects of extrinsic relaxation often used in the analysis of dynamic conductivities of ionically conducting glasses. The dielectric modulus ($M^* = 1/\varepsilon^*$) is frequently used in the analysis of dielectric data of ionic conductors [32]. The advantage of adopting complex electrical modulus spectra is that it can discriminate against electrode polarization and grain boundary conduction process which the CIS is unable to do. Using electric modulus analysis, it is easier to relate this phenomenon to other properties, especially the dynamical mechanical modulus and it can be written as a single function of conductivity. Sinclair and West [33,34] suggested the combined usage of impedance and modulus spectroscopic plots to rationalize the dielectric properties. Thus, the power of combined usage of both impedance and modulus spectroscopy is that the Z'–Z'' plot highlights the phenomenon with the largest resistance whereas M'' vs. M' picks up those of the smallest capacitance [35]. The imaginary parts of the impedance and electric modulus are expressed as:

$$Z'' = R\frac{\omega \cdot R \cdot C}{1 + (\omega \cdot R \cdot C)^2} \tag{1a}$$

$$M'' = \frac{C_0}{C} \cdot \frac{\omega \cdot R \cdot C}{1 + (\omega \cdot R \cdot C)^2} \tag{1b}$$

The peaks in the spectra of $\log Z''$ or $\log M''$ plotted against $\log f$ appear at the same frequency (f) and are derived by:

$$\omega_{max} = \frac{1}{R \cdot C} = \tau^{-1} \tag{2}$$

From the above Eqs. 1 and 2, the peak values of the imaginary parts of the impedance and electric modulus are given as:

$$Z''_{max} = \frac{R}{2} \tag{3a}$$

$$M''_{max} = \frac{C_0}{2C} \tag{3b}$$

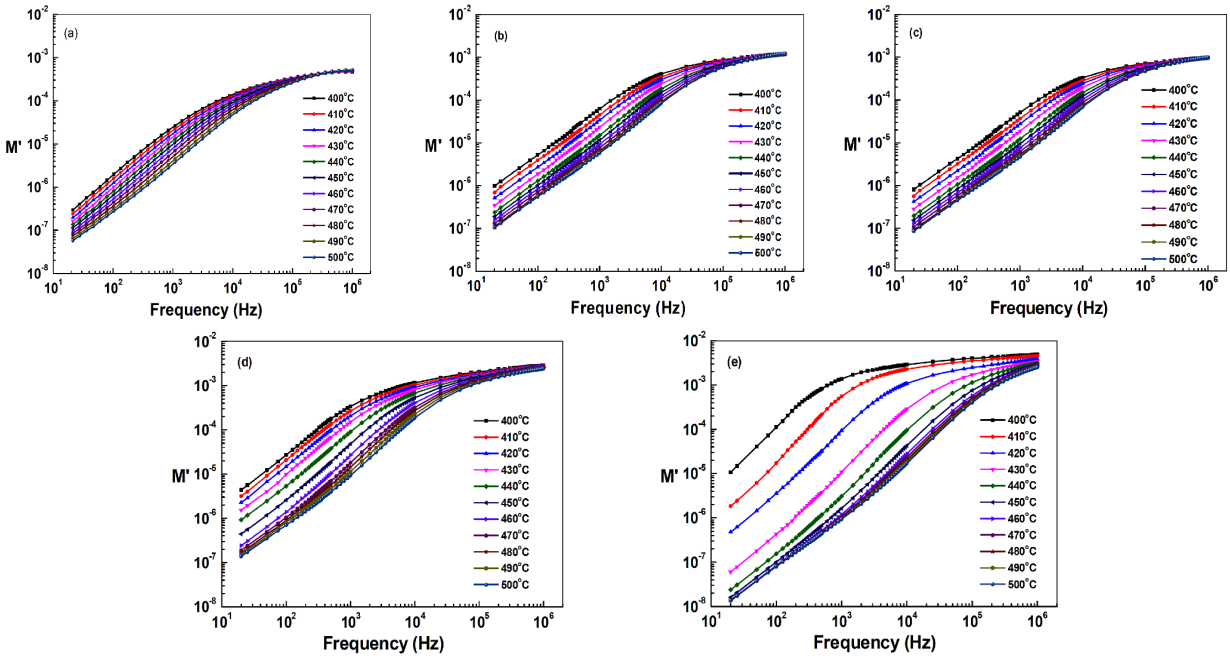

Figure 6. Frequency dependence of M' for $(Bi_{0.5}Na_{0.5})_{0.94}Ba_{0.06}Ti_{1-x}(Mg_{1/3}Nb_{2/3})_xO_3$, where x is: a) 0, b) 0.25, c) 0.50, d) 0.75 and e) 1.00 at temperatures up to 500 °C

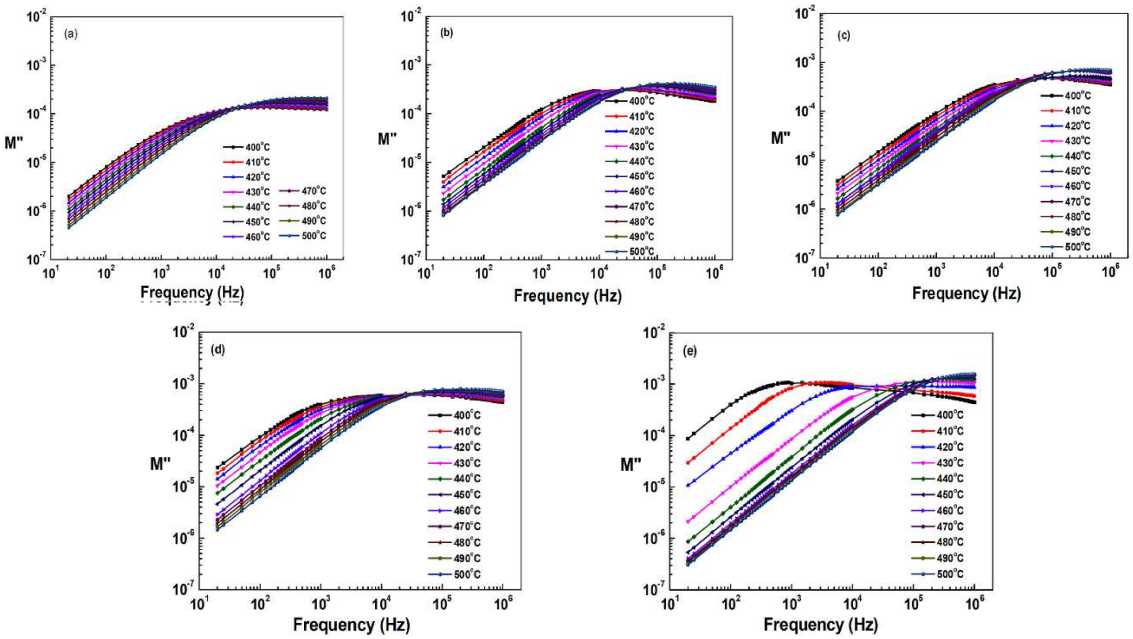

Figure 7. Frequency dependence of M'' for $(Bi_{0.5}Na_{0.5})_{0.94}Ba_{0.06}Ti_{1-x}(Mg_{1/3}Nb_{2/3})_xO_3$, where x is: a) 0, b) 0.25, c) 0.50, d) 0.75 and e) 1.00 at temperatures up to 500 °C

The frequency dependence of $M'(\omega)$ and $M''(\omega)$ for all the BNBT-MN_x materials at various temperatures is shown in Figs. 6 and 7. $M'(\omega)$ plots show a dispersion tending toward M_∞ (the asymptotic value of $M'(\omega)$ at higher frequencies, while $M''(\omega)$ plots exhibit a maximum (M''_{max}) centred at the dispersion region of $M'(\omega)$. The frequency range below the peak frequency determines the frequency range in which charge carriers are mobile over a long distance whereas, in the frequency range above the peak frequency, the charge carriers are confined to the potential wells and are mobile over short distances [36]. The value of M'' increases with increasing temperature, though slightly, and shifts to the higher frequency side. An increase in the peak height of M'' was observed with increasing temperature, which is indicative of a decrease in the capacitance with increasing temperature and is a characteristic feature of a ferroelectric material in the paraelectric region above T_C. The peaks were also found to shift systematically towards higher frequency with an increase in temperature as shown in Fig. 7. It suggests a hopping conduction mechanism in the investigated BNBT-MN_0, BNBT-$MN_{0.25}$, BNBT-$MN_{0.50}$, BNBT-$MN_{0.75}$ and BNBT-$MN_{1.00}$ ceramic compositions. However, an opposite trend of variation in $M''(\omega)$, i.e. a decrease in the peak height of M'' was observed with increasing temperature for BNBMN corresponding to 400, 410 and 420 °C as shown in Fig. 7e.

Complex modulus spectrum ($M''(\omega)$ vs. $M'(\omega)$) for BNBT-MN_0, BNBT-$MN_{0.25}$, BNBT-$MN_{0.50}$, BNBT-$MN_{0.75}$ and BNBT-$MN_{1.00}$ ceramic compositions at different indicated temperatures from 400 to 500 °C are shown in Fig. 8. In these figures, one can notice that spectra for all the samples have typical semicircular patterns with their centres lying below the real axis (indicating non-Debye type of relaxation response) similar to the corresponding complex impedance plots. In the latter case the depressed semicircles corresponding to grains (group of right semicircles representing data corresponding to higher frequencies for each set) and grain boundaries (group of left semicircles representing data corresponding to lower frequencies for each set) are clearly visible. Larger semicircles for the grains and smaller ones for the corresponding grain boundaries in each of the plots in Fig. 8 show the dominance of grains over the grain boundaries in each of the given compositions at the measurement temperatures ranging from 400 °C to 500 °C.

The frequency spectra of AC conductivity for BNBT-MN_0, BNBT-$MN_{0.25}$, BNBT-$MN_{0.50}$, BNBT-$MN_{0.75}$ and BNBT-$MN_{1.00}$ ceramics at different measuring temperatures are shown in Fig. 9. The AC conductivity shows dispersion with the increase of temperature at lower frequencies, which is more pronounced for the doped samples. The plots reveal that σ_{AC} decreases with decreasing frequency, but at higher temperatures (~500 °C) it is observed that σ_{AC} becomes almost independent of frequency in low frequency region. Thus, extrapolation of this part towards lower frequency gives DC conductivity.

The value of σ_{AC} increases with the increasing temperature, thereby clearly indicating the negative temperature coefficient of resistance (NTCR) character of the samples. The value of σ_{AC} is seen to increase also with increasing values of x. The apparent activation energy was obtained using the Arrhenius relationship:

$$\sigma_{AC} = \sigma_0 \cdot \exp\left(-\frac{E_a}{k_B \cdot T}\right) \tag{4}$$

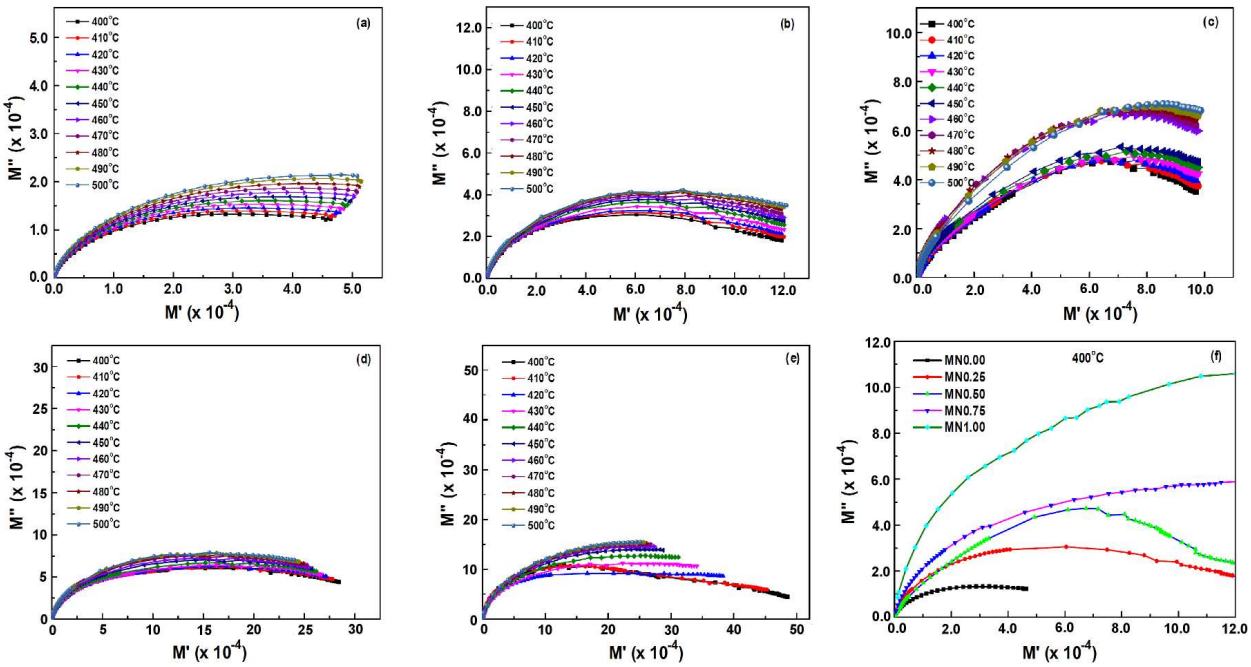

Figure 8. Complex electric modulus plots for $(Bi_{0.5}Na_{0.5})_{0.94}Ba_{0.06}Ti_{1-x}(Mg_{1/3}Nb_{2/3})_xO_3$ (where x is: a) 0, b) 0.25, c) 0.50, d) 0.75 and e) 1.00) from 400 to 500 °C at different indicated temperatures. Figure (f) shows the complex modulus plots for the five compositions at 400 °C

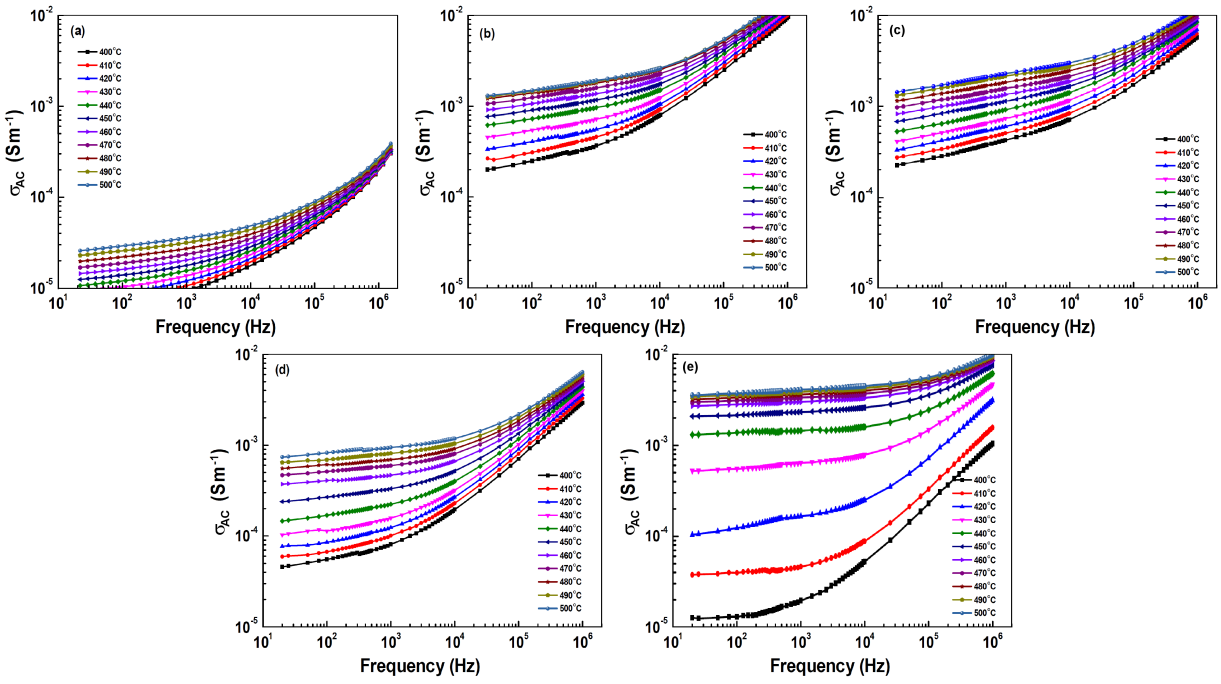

Figure 9. Frequency dependence of the real part of complex AC conductivity (σ_{AC}) for $(Bi_{0.5}Na_{0.5})_{0.94}Ba_{0.06}Ti_{1-x}(Mg_{1/3}Nb_{2/3})_xO_3$ (where x is: a) 0, b) 0.25, c) 0.50, d) 0.75 and e) 1.00) from 400 to 500 °C

For the variation of $\ln \sigma_{AC}$ versus $10^3/T$, a linear least squares fitting of the AC conductivity data at 1 kHz between temperature limits of 400–500 °C gives the values of the apparent activation energy, E_a, to be 0.330, 0.801, 0.791, 1.206, and 2.037 eV for x = 0, 0.25, 0.50, 0.75 and 1.00, respectively. Hence, the apparent activation energy is seen to increase with increasing $(Mg^{2+}_{1/3}Nb^{5+}_{2/3})$ content in the fabricated ceramics. The low value of E_a supports the hopping type of charge carriers' transport in the investigated materials between localized states in a random manner.

IV. Conclusions

Lead free ceramics $(Bi_{0.5}Na_{0.5})_{0.94}Ba_{0.06}Ti_{1-x}(Mg_{1/3}Nb_{2/3})_xO_3$ (x = 0, 0.25, 0.50, 0.75 and 1.00) were fabricated using solid state reaction technique. Rietveld refinements of XRD data revealed that

$(Bi_{0.5}Na_{0.5})_{0.94}Ba_{0.06}TiO_3$ as well as the compositions up to $x = 0.50$ have monoclinic structure with space group $P2/m$ whereas $(Bi_{0.5}Na_{0.5})_{0.94}Ba_{0.06}Ti_{1-x}(Mg_{1/3}Nb_{2/3})_xO_3$ ($x = 0.75$ and 1.00) have tetragonal (pseudo-cubic) structures with space group $P4/mmm$. Thus, incorporation of pseudo-cation $(Mg^{2+}_{1/3}Nb^{5+}_{2/3})$ in place of Ti^{4+} at the B-site of BNBT matrix resulted in the change of unit cell structure from monoclinic to the tetragonal structure.

The frequency and temperature dependent complex impedance/modulus, as well as AC conductivity data, indicated the dominance of semiconducting grains showing NTCR behaviour and distribution of relaxation times with a clear cut departure from the ideal Debye type behaviour. The variation of $\ln \sigma_{AC}$ versus $10^3/T$ revealed that the value of σ_{AC} increases with the increasing temperature, thereby endorsing the NTCR character of the samples. On the other hand, the value of σ_{AC} is seen to decrease with increasing values of x. It should be added that the investigation of piezoelectric properties of the fabricated ceramics is in progress and will be reported in near future.

References

1. J.F. Tressler, S. Alkroy, R.E. Newnham, "Piezoelectric sensors and sensor materials", *J. Electroceram.*, **2** (1998) 257–272.
2. M.E. Lines, A.M. Glass, *Principles and Applications of Ferroelectrics and Related Materials*, Clarendon Press, Oxford, 1977.
3. G.A. Smolenskii, V.A. Isupov, A.I. Agranovskaya, N. Kraink, "New ferroelectrics of complex composition", *Sov. Phys. Solid State*, **2** (1961), 2651–2654.
4. D.Z. Zhang, Z. Zhenga, X. Feng, T. Zhang, J. Sun, S.H. Dai, L.J. Gong, Y.Q. Gong, L. He, Z. Zhu, J. Huang, X. Xu, "Ferro-piezoelectric properties of $0.94(Na_{0.5}Bi_{0.5})TiO_3$-$0.06BaTiO_3$ thin film prepared by metal-organic decomposition", *J. Alloys Compd.*, **504** (2010) 129–133.
5. N. Ichinose, K. Udagawa, "Piezoelectric properties of $(Bi_{1/2}Na_{1/2})TiO_3$ based ceramics", *Ferroelectrics*, **169** (1995) 317–325.
6. J. Suchanicz, M.G. Gavshin, A.Y. Kudzin, C. Kus, "Dielectric properties of $(Na_{0.5}Bi_{0.5})_{1-x}Me_xTiO_3$ ceramics near morphotropic phase boundary", *J. Mater. Sci.*, **36** (2001) 1981–1985.
7. G.O. Jones, P.A. Thomas, "Investigation of the structure and phase transitions in the novel A-site substituted distorted perovskite compound $Na_{0.5}Bi_{0.5}TiO_3$", *Acta Crystallogr. B*, **58** (2002) 168–178.
8. T. Takenaka, K. Maruyama, K. Sakata, "$(Bi_{1/2}Na_{1/2})TiO_3$-$BaTiO_3$ system for lead-free piezoelectric ceramics", *Jpn. J. Appl. Phys.*, **30** (1991) 2236–2239.
9. Y. Li, W. Chen, J. Zhou, Q. Xu, H. Sun, R. Xu. "Dielectric and piezoelectric properties of lead-free $(Bi_{0.5}Na_{0.5})TiO_3$-$NaNbO_3$ ceramics", *Mater. Sci. Eng. B*, **112** (2004) 5–9.
10. T. Takenaka, K. Sakata, "Piezoelectric properties of $(Bi_{1/2}Na_{1/2})TiO_3$-based ceramics", *Ferroelectrics*, **106** (1990) 375–380.
11. Y.M. Li, W. Chen, Q. Xu, J. Zhou, X. Gu, "Piezoelectric and ferroelectric properties of $(Bi_{0.94-x}La_xNa_{0.94})_{0.5}Ba_{0.06}TiO_3$ lead-free ceramics", *J. Phys. D: Appl. Phys.*, **41** [12] (2008) 125411.
12. B.J. Chu, D.R. Chen, G.R. Li, Q.R. Yin, "Electrical properties of $Na_{1/2}Bi_{1/2}TiO_3$-$BaTiO_3$ ceramics", *J. Eur. Ceram. Soc.*, **22** (2002) 2115–2121.
13. A.K. Roy, A. Singh, K. Kumari, K. Amaranth, A. Prasad, K. Prasad, "Electrical properties and ac conductivity of $(Bi_{0.5}Na_{0.5})_{0.94}Ba_{0.06}TiO_3$ ceramic", *ISRN Ceramics*, **2012** (2012) 854831.
14. H.D. Li, C.D. Feng, W.L. Yao, "Some effects of different additives on dielectric and piezoelectric properties of $(Bi_{1/2}Na_{1/2})TiO_3$-$BaTiO_3$ morphotropic-phase-boundary composition", *Mater. Lett.*, **58** (2004) 1194–1198.
15. Y.M. Li, W Chen, Q. Xu, J. Zhou, H.J. Sun, R. Xu, "Dielectric and piezoelectric properties of $Na_{0.5}Bi_{0.5}TiO_3$-$K_{0.5}Bi_{0.5}TiO_3$-$NaNbO_3$ lead-free ceramics", *J. Electroceram.*, **14** (2005) 53–58.
16. R. Zuo, X. Fang, C. Ye, "Phase structures and electrical properties of new lead-free $(Na_{0.5}K_{0.5})NbO_3$-$(Bi_{0.5}Na_{0.5})TiO_3$ ceramics", *Appl. Phys. Lett.*, **90** (2007) 092904.
17. H. Du, W. Zhou, D. Zhu, L. Fa, S. Qu, Y. Li, Z. Pei, "Sintering characteristic, microstructure, and dielectric relaxor behavior of $(K_{0.5}Na_{0.5})NbO_3$-$(Bi_{0.5}Na_{0.5})TiO_3$ lead-free ceramics", *J. Am. Ceram. Soc.*, **91** (2008) 2903–2909.
18. Y.M. Li, W. Chen, J. Zhou, "Dielectric and ferroelectric properties of lead-free $Na_{0.5}Bi_{0.5}TiO_3$-$K_{0.5}Bi_{0.5}TiO_3$ ferroelectric ceramics", *Ceram. Int.*, **31** (2005) 139–142.
19. C. Peng, J.F. Li, W. Gong, "Preparation and properties of $(Bi_{1/2}Na_{1/2})TiO_3$-$Ba(Ti,Zr)O_3$ lead-free piezoelectric ceramics", *Mater. Lett.*, **59** (2005) 1576–1580.
20. L. Gao, Y. Huang, L. Liu, T. Liu, C. Liu, F. Zhou, X. Wan, "Crystal structure and properties of $BaTiO_3$-$(Bi_{0.5}Na_{0.5})TiO_3$ ceramic system", *J. Mater. Sci.*, **43** (2008) 6267–6271.
21. H. Nakada, N. Koizumi, T. Takenaka, "Lead-free piezoelectric ceramics of $(Bi_{1/2}Na_{1/2})TiO_3$-$BiFeO_3$ system", *Key Eng. Mater.*, **169-170** (1999) 37–40.
22. X. Wang, H.L. Chan, C. Choy, "Piezoelectric and dielectric properties of CeO_2-added $(Bi_{0.5}Na_{0.5})_{0.94}Ba_{0.06}TiO_3$ lead-free ceramics", *Solid State Commun.*, **125** (2003) 395–399.
23. J.J. Hao, X.H. Wang, Z.L. Gui, L.T. Li, "Effect of MnO_2 on the property of bismuth sodium titanate piezoelectric ceramics", *Rare Metal Mater. Eng.*, **32** (2003) 438–440.
24. A. Herabut, A. Safari, "Processing and electromechanical properties of $(Bi_{0.5}Na_{0.5})_{(1-1.5x)}La_xTiO_3$ ceramics", *J. Am. Ceram. Soc.*, **80** (1997) 2954–2958.
25. A. Watcharapasorn, S. Jiansirisomboon, T. Tunkasiri, "Sintering of Fe-doped $Bi_{0.5}Na_{0.5}TiO_3$ at <1000 °C", *Mater. Lett.*, **61** (2007) 2986–2989.
26. H. Wang, R. Zuo, Y. Liu, J. Fu, "Densification behavior, microstructure, and electrical properties of sol-gel-derived niobium-doped $(Bi_{0.5}Na_{0.5})_{0.94}Ba_{0.06}TiO_3$ ceramics", *J. Mater. Sci.*, **45** (2010) 3677–3682.
27. S.K. Roy, S.N. Singh, S.K. Mukherjee, K. Prasad, "$Ba_{0.06}(Na_{1/2}Bi_{1/2})_{0.94}TiO_3$-$Ba(Fe_{1/2}Ta_{1/2})O_3$: giant permittivity lead-free ceramics", *J. Mater. Sci. Mater. Electron.*, **28** (2017) 4763–4771.
28. S.K. Roy, S. Chaudhuri, R.K. Kotnala, D.K. Singh, B.P. Singh, S.N. Singh, K.P. Chandra, K. Prasad, "Dielectric and Raman studies of $Ba_{0.06}(Na_{1/2}Bi_{1/2})_{0.94}TiO_3$-$NaNbO_3$

ceramics", *Mater. Sci. Poland*, **34** (2016) 437–445.
29. S.K. Roy, S.N. Singh, K. Prasad, "Structure, microstructure and infrared studies of $Ba_{0.06}(Na_{1/2}Bi_{1/2})_{0.94}TiO_3$-$NaNbO_3$ ceramics", *AIP Conf. Proc.*, **1728** (2016) 020217.
30. E.A. Zereffa, A.V.P. Rao, "Effect of simultaneous substitution of magnesium and niobium on dielectric properties and phase transition temperature of bismuth sodium barium titanate ceramics", *Mater. Sci. Poland*, **31** (2013) 201–210.
31. S. Sen, R.N.P. Choudhary, A. Tarafdar, P. Pramanik, "Impedance spectroscopy study of strontium modified lead zirconate titanate ceramics", *J. Appl. Phys.*, **99** (2006) 124114.
32. N.G. McCrum, B.E. Read, G. Williams, *Anelastic and Dielectric Effects in Polymeric Solids*, Wiley & Sons, New York, 1967.
33. D.C. Sinclair, A.R. West, "Impedance and modulus spectroscopy of semiconducting $BaTiO_3$ showing positive temperature coefficient of resistance", *J. Appl. Phys.*, **66** (1989) 3850–3856.
34. D.C. Sinclair, A.R. West, "Effect of atmosphere on the PTCR properties of $BaTiO_3$ ceramics", *J. Mater. Sci.*, **29** (1994) 6061–6068.
35. K.S. Rao, K.V. Rajulu, B. Tilak, A. Swathi, "Effect of Ba^{2+} in BNT ceramics on dielectric and conductivity properties", *Nat. Sci.*, **2** (2010) 357–367.
36. S.K. Barik, R.N.P. Choudhary, A.K. Singh, "AC impedance spectroscopy and conductivity studies of $Ba_{0.8}Sr_{0.2}TiO_3$ ceramics", *Adv. Mater. Lett.*, **2** (2011) 419–421.